Cement and Concrete Research 124 (2019) 105804

Contents lists available at ScienceDirect

Cement and Concrete Research

journal homepage: www.elsevier.com/locate/cemconres

Tensile response of low clinker UHPFRC subjected to fully restrained shrinkage

Mohamed Abdul Hafiz*, Amir Hajiesmaeili, Emmanuel Denarié

Laboratory of Maintenance and Safety of Structures, MCS-IIC-ENAC, EPFL - Ecole Polytechnique Fédérale de Lausanne, CH-1015 Lausanne, Switzerland

ARTICLE INFO

Keywords:
UHPFRC
Restrained shrinkage
TSTM
Isothermal calorimetry
VRFT
Early age
Low clinker
Limestone filler

ABSTRACT

This paper addresses the tensile response of Strain Hardening Ultra High Performance Fiber Reinforced Concretes (SH-UHPFRC) subjected to restrained autogenous shrinkage deformations under full and partial restraint conditions, right after casting and until one month. The development of autogenous shrinkage and corresponding eigenstresses under various degrees of restraint were studied for two types of mixes; Mix I with type I cement and silica fume, and Mix II with silica fume and 50% mass replacement of type I cement with limestone filler. The tests under 100% restraint conditions are the first of their kind on SH-UHPFRC and the results show that under these conditions, the material enters into the strain-hardening domain of the tensile response. The development of eigenstresses was much slower in the Mix II when compared to that of Mix I. The development of the dynamic elastic modulus and heat of hydration were also studied and put into perspective.

1. Introduction

Ultra High Performance Fiber Reinforced Concretes (UHPFRC) are cementitious materials with very low permeability, outstanding durability and excellent mechanical properties. They have high tensile strength and exhibit significant strain hardening behavior (1–5‰) with a suitable fibrous mix. Because of these outstanding properties, they are very well adapted for the improvement of load carrying capacity and protective functions of existing structures [1].

In composite UHPFRC-concrete structures, a UHPFRC reinforcing and/or protective layer is applied on an existing structure. The UHPFRC layer undergoes intensive early age volume changes due to hydration reactions; thermal effects (more or less pronounced depending on the UHPFRC layer thickness), autogenous shrinkage and to some extent drying shrinkage if the UHPFRC layer remains exposed to the outside. It should also be noted that these deformations, especially the drying shrinkage, not only act in the early age, but can also occur over longer spans of time. These deformations are restrained by the existing structure as well as the reinforcement bars in the UHPFRC layer, if any, which will lead to the development of tensile eigenstresses in the UHPFRC layer [2–4]. The stiffness of the existing structure will affect the degree of restraint imposed by the structure, which in turn affects the value of the eigenstresses developed. Denarié et al. [5] showed that depending on the stiffness of the structure, even >90% of the free deformations can be restrained, leading to conditions which are close to full restraint.

Only a few works have been carried out to study restrained shrinkage and the associated eigenstresses development in UHPC [6,7] and in UHPFRC [2,3,8–11]. The effect of shrinkage reducing admixtures and superabsorbent polymers on the early age shrinkage of UHPC was investigated in [12,13]. The effect of specimen thickness on the restrained shrinkage behavior of UHPFRC was studied in [10,11] and it was shown that the cracking risk is reduced as the thickness of the specimen increase. However, to the best of the authors' knowledge, no extensive research has been reported in open literature on the influence of full restraint conditions on the development of the eigenstresses in UHPFRC.

The strain hardening capacity of UHPFRC helps to mitigate the detrimental effects of the eigenstresses, except in very special cases of unfavorable fiber orientations, in which case the strain hardening response is limited or lost and the eigenstresses may lead to premature localized cracking, with reduced protective performance. The viscoelastic potential in tension of the UHPFRC also helps to relax the developed eigenstresses, thereby reducing their adverse effects. However, depending on the stress level, the relaxation may be associated to linear viscoelastic or non-linear viscoelastic. Kamen et al. [14] showed that UHPFRC viscous response at early age (3 days) deviates considerably from a linear response when the tensile stress level changes from 32% to 63% of the tensile strength. Because of the interaction of various complex effects like the hydration and ageing, stress level, loading

* Corresponding author.
E-mail address: mohamed.hafz@epfl.ch (M.A. Hafiz).

https://doi.org/10.1016/j.cemconres.2019.105804
Received 15 January 2019; Received in revised form 27 June 2019; Accepted 27 June 2019
Available online 16 July 2019

history and their couplings, the time dependent behavior of UHPFRC at early age under high sustained loads is not fully understood.

Only a few studies have been carried out to understand the viscoelastic behavior of UHPFRC in compression [3,15–20] and in tension [8,19,21–23]. It was shown that the compressive creep response of UHPFRC is significantly lower than that of ordinary concretes at a similar loading age and load level [24]. The basic compressive creep coefficient of UHPFRC without thermal treatment, at a loading age of 28 days, for a load level below 40% of the compressive strength, is typically 0.8–1, instead of 2–4 for normal concretes [24]. [25–27] studied the early age tensile creep behavior of concrete and [28] showed that the viscous properties of concrete help to reduce the cracking tendency by reducing the early age eigenstresses by about 50%. [2,8] showed that the response was similar in UHPFRC. Very few studies have been conducted to understand the early age tensile creep of UHPFRC [4,14,29,30]. The TSTM setup developed at MCS-EPFL by Kamen et al. [2,8] was used extensively to investigate the early age tensile response of Strain hardening UHPFRC under various temperatures and loading conditions, which confirmed a significant creep potential for the material due to its high paste volume [9,21].

In these mixes, because of the low w/c ratio, the overall degree of hydration is much less (about 30% to 40% at 28 days) than that of normal concretes [9]. Because of this, it is advantageous to replace a part of the unhydrated clinker with Supplementary Cementitious Materials (SCMs) like limestone filler. No work has been carried out until now to study the development of autogenous deformations and eigenstresses under restraint for UHPFRC mixes with massive replacement of clinker with limestone fillers. Powers et al. [31] showed that complete hydration of cement can occur only for water/binder ratios of 0.42 in the long term. Waller [32] and Jensen [33] extended this model to systems with silica fume. Using these models, [8,9,34] predicted the maximum degree of hydration of cement in different types of UHPFRC and showed that it is low, around 30% to 50%. Thus if cement (clinker) is progressively replaced by inert particles in a UHPC matrix, such that the overall amount of hydrates stays the same, no detrimental consequences on the mechanical performance of the material should be observed. This effect was shown by many researchers for normal and high strength concrete [6,35,36]. [37] studied combinations of limestone filler, cement and silica fume in high performance mortars with cement replacement by filler up to 25% mass. [38–43] showed that it is possible to replace significant amounts of cement in UHPC mixes with low w/b ratios (0.19–0.25) with fillers like fly ash, limestone filler, GGBS and metakaolin, keeping the w/b ratio constant, without significantly decreasing the compressive strength. The same trend was observed by [44,45] with clinker replacement by limestone filler in SH-UHPFRC mixes. Ghafari et al. [46] discusses the effect of SCMs such as FA and GGBS on the porosity and autogenous shrinkage of UHPC. They show that the full or partial replacement of SF by the SCMs lead to a considerable decrease in the finer pores and thereby lead to lower autogenous shrinkage, without much loss in the compressive strength. Schachinger et al. [7] showed that the autogenous deformations in blast furnace cement concretes were lower than that with normal OPC; with values of 0.6‰ and 1.3‰ respectively after 1 day and 1.3‰ and 1.7‰ respectively after 56 days. [47] showed that the autogenous shrinkage of RPC can be effectively mitigated by addition of SCMs like GGBS along with internal curing by means of super absorbent polymers. Even though many reporters report a decrease in the autogenous shrinkage with the replacement of fillers in UHPC (w/b = 0.19–0.25) [46–49], some reporters indicate an increase in the autogenous shrinkage with the addition of GGBS as a filler [48]. [42] showed that the shrinkage of HPC with FA or GGBS reduced by 14.28% and 27.95% respectively at 180 days and that the creep at 180 days reduced by 36.71% and 56.11% respectively, when compared to standard mix with only cement. The knowledge on the shrinkage and creep of UHPFRC with SCMs, along with the development of eigenstresses under restrained shrinkage is scarce in literature. Moreover, according to the best of the authors' knowledge, very few studies have been made to understand the tensile properties of UHPFRC with SCMs like limestone filler, fly ash or GGBS [50].

In the present paper, the eigenstresses development in UHPFRC under full and partial restraint conditions will be investigated for two types of UHPFRC mixes; Mix I with type I cement and silica fume, and Mix II with 50% mass replacement of type I cement with limestone filler. The development of autogenous deformations in these mixes will be studied from the time of casting until one month or more. Vibration Resonance Frequency Tests (VRFT) will be carried out to study the development of dynamic elastic modulus of the two mixes. Isothermal calorimetry tests will also be conducted to understand the kinetics of overall hydration of the mixes.

2. Experimental

2.1. Materials and preparation

Two mixes were used for the present study, both from the $CEMTEC_{multiscale}$© family. The $CEMTEC_{multiscale}$© mixes were initially developed at Laboratoire Central des Ponts et Chaussées (LCPC), France [51]. This mix was optimized and modified in the framework of the research works held in MCS/EPFL for rehabilitation and strengthening of existing structures [44,52] to produce Mix I, which is a UHPFRC type CM22_TKK_b. The matrix is composed of cement (CEM I 52.5 HTS from Le Teil, Lafarge), white microsilica (SEPR, BET = 14 m^2/g), superplasticizer (Cementol Zeta Super S from TKK, Slovenia) and water. The matrix is a pure cement paste with no fine sand, to accommodate all the fibers and therefore exhibits excellent rheological properties in the fresh state even though the water/binder ratio is very low, 0.129.

Since the degree of hydration of cement in Mix I is only 30% after 28 days [9], it was decided to replace 50% of the cement with inert limestone filler. The mix, which will be designated as Mix II from here on, contains two types of limestone fillers: Betoflow D® and Betocarb SL® (OMYA), of different gradings. Both mixes were developed based on the concept of packing density, which is the key for obtaining Ultra high-performance cementitious composites. The total water added to the system is divided into two main parts; the void water which is the amount of water needed to fill the voids and the excess water which is the rest of the water that gives workability to the mix. Optimizing the packing density with the help of different grain size classes, reduces the voids in the matrix and therefore the void water, thereby improving the overall workability-strength performance of the cementitious material. In this study, the generalized CIPM model [53,54] was implemented to optimize the packing density of the mixes. The water film thickness, which is the amount of excess water divided by the surface area of the particle system, was kept similar in both mixes, in order to have two comparable mixes with similar workability. Fig. 1 shows the particle size distribution (PSD) of the individual components used in the formulation of the matrix together with that of the final mixes. The overall PSD of the final mixes were obtained from the mix-design and the PSD of the individual components, which were determined using laser diffraction. More details regarding the procedure adopted for optimizing the packing density could be found in [54].

Both mixes had a fibrous mix containing two types of steel fibers; microfibers and macrofibers, with a total dosage of 9% by volume after the concepts developed by Rossi et al. [51]. The microfibers (steel wool, from Gervois, France) had a semi-circular section with variable dimensions and an irregular aspect ratio. The macrofibers were straight with l_f = 10 mm, d_f = 0.2 mm and turned out to be slightly torqued after the cutting process of the original wires, produced by Redaelli TECNA, Italy. Both mixes exhibit a significant strain hardening behavior under tension (1–2‰) [21,55,56]. The detailed compositions of Mix I and II along with those of the corresponding UHPC matrices (without fibers, designated as Mix I_m and Mix II_m) are given in Table 1. The chemical and physical properties of the cement and silica fume

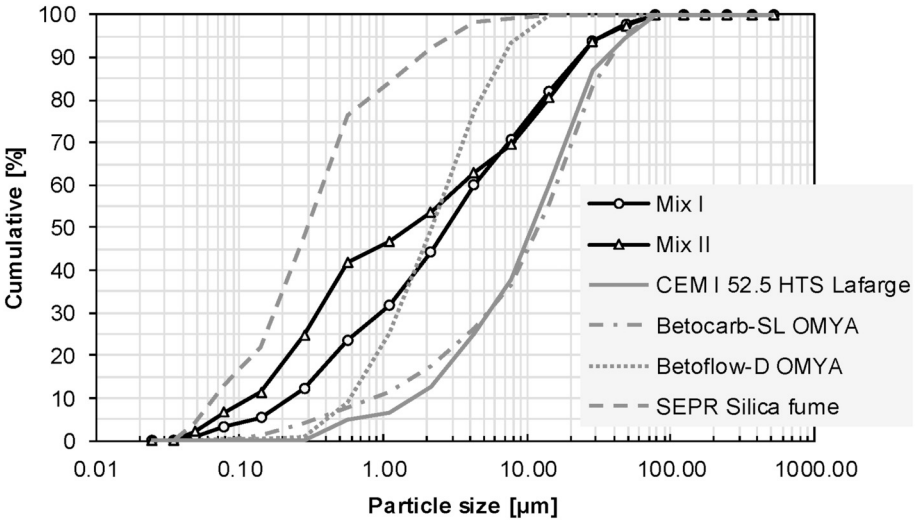

Fig. 1. Particle size distribution of the mixes along with that of the individual components.

used are given in Table 2.

The procedure for mixing the components was the same for both mixes. Initially the powders (cement, silica fume, limestone fillers) and the microfibers were mixed for 3 min. Water was then added to the mix, while the superplasticizer was added 1 min after. The entire composition was mixed for 7–8 min after which 50% of the total steel fibers were added and mixed for 45 s. The remaining 50% of the fibers were then added and the whole mix was mixed for another 2 min. At the end of mixing, the workability of the mixes was tested following ASTMC1437 [57]. The air content as well as the specific gravity of the mixes were also measured using an air content meter after EN 459-2. The properties of both mixes in the fresh state are shown in Table 3 and that in the hardened state are shown in Table 4.

The compressive strength and modulus of elasticity were determined on 70 mm × 140 mm cylinders, whereas the tensile properties were obtained from uniaxial tensile tests at a strain rate of 10^{-5} 1/s, on dumbbell specimens with a center cross section of 50 mm × 30 mm, following [58]. The sorptivity was also measured for both mixes at an age of 28 days following EN 1925: 99-07.

2.2. Vibration Resonance Frequency Test (VRFT)

The development of the dynamic moduli of elasticity of the two mixes was studied using the Vibration Resonance Frequency Test method. The automatic test setup for two specimens in parallel was developed by [59] in EPFL following the works of Kazemi Kamyab [9], after [60]. The tests were carried out on two cylindrical specimens 140 mm in length and 70 mm in diameter, inside a climate room maintained at 20 °C ± 1 °C. The specimens were weighed and the

Table 2
Chemical compositions of cement and SF_{SEPR}.

Components	Chemical composition (%)	
	Cement	SF_{SEPR}
SiO_2	22.75	94
TiO_2	-	< 500 ppm
Al_2O_3	2.7	3
Fe_2O_3	1.9	0.15
CaO	67.1	0.02
Na_2O	0.15	0.10
K_2O	0.2	0.06
MgO	0.75	-
SO_3	2.1	60 ppm
ZrO_2	-	2.4
P_2O_5	0.2	-
Cl	< 0.1	-
C	-	40 ppm
CO_2	1.3	-

Table 3
Properties of Mix I and II in the fresh state (average value from 4 tests).

Property	Units	Mix I	Mix II
Workability (ASTM - spread after 25 blows)	mm	179	146
Specific weight	kg/m^3	2834	2695
Air content	%	3.2	4.7

Table 1
Compositions of Mix I and II.

Material	Units	Mix I	Mix II	Mix I_m*	Mix II_m*
		[kg/m^3]	[kg/m^3]	[kg/m^3]	[kg/m^3]
Cement, CEM I 52.5 le Teil	[kg/m^3]	1467.0	733.7	1616.2	809.6
Silica fume, SEPR	[kg/m^3]	381.4	293.5	420.2	323.8
Limestone filler 1 (Betocarb SL®)	[kg/m^3]	–	223.0	–	246.1
Limestone filler 2 (Betoflow D®)	[kg/m^3]	–	510.6	–	563.4
Steel fibers (straight macro fibers; l_f = 10 mm, d_f = 0.2 mm and microfibers/steel wool)	[kg/m^3]	706.5	706.5	–	–
Total water	[kg/m^3]	225.8	217.9	248.7	240.4
Superplasticizer from TKK, Slovenia; Zementol zeta super S; polycarboxylate; 25% solid content; (total amount)	[kg/m^3]	20.5	14.7	22.6	16.2
Packing density	[–]	0.815	0.793	–	–

* Compositions of the UHPC matrix without fibers.

Table 4
Properties of Mix I and II in the hardened state.

Property	Units	Mix I	Mix II	Age (days)
Tensile first crack strength* (average of 8 tests)	MPa	12.3 ± 1.7	11.1 ± 1.9	14
Uniaxial tensile strength (average of 8 tests)	MPa	18.0 ± 3.1	15.1 ± 2.7	14
Modulus of elasticity in tension (average of 8 tests)	GPa	51.0 ± 2.3	46.3 ± 1.3	14
End of tensile hardening (average of 10 tests)	‰	1.6 ± 0.4	1.3 ± 0.5	14
Compressive strength (average of 3 tests)	MPa	230.5 ± 0.9	169.7 ± 0.5	28
Modulus of elasticity in compression (average of 3 tests)	GPa	48.3 ± 0.8	46.3 ± 0.8	28
Sorptivity (average of 2 tests)	$gr/m^2\sqrt{h}$	45.0 ± 5.2	32.5 ± 9.5	28

* Transition from the elastic behavior to the strain hardening behavior.

surfaces were sealed with two layers of aluminum tape in order to prevent the drying and moisture loss. The cylinders were then kept on a support in front of a system consisting of a steel ball suspended using a steel thread. The specimens were hit at their centers, at one end, with the steel ball, that produced longitudinal vibrations in the specimens, which were measured using an accelerometer fixed on the other end of the cylinder. The data acquisition was done at a rate of one measurement per minute.

Using an analytical procedure developed by [60], the dynamic elastic modulus was determined at different ages. The proposed analytical procedure was based on a three-dimensional analysis of the vibration of the cylinder. The two first longitudinal resonance frequencies were determined, from which the elastic modulus and Poisson's ratio were calculated at the different ages investigated.

2.3. Isothermal calorimetry tests

Isothermal calorimetry tests were done in a TAM AIR calorimeter from TA instruments, and the heat flow in the mixes was continuously measured from the time of casting, to follow the kinetics of hydration. The thermostat in the TAM AIR can maintain the temperature in the samples and the surrounding environment within ±0.02 °C of the chosen isothermal temperature. The mixes used for the isothermal calorimetry tests did not have the micro or macro fibers. Four samples were tested for each of Mix I_m and Mix II_m at 20 °C. Immediately after mixing, about 10 g of the sample was placed into a 20 mL glass ampoule and kept in the calorimeter, along with a reference sample of water in another ampoule, which acted as an inert sample to improve the signal to noise ratio and identify the temperature artefacts and fluctuations. More detailed information regarding the test procedure and sample preparation could be found in [61,62].

2.4. Temperature Stress Testing Machine (TSTM)

The Temperature Stress Testing Machine was developed at MCS/EPFL during the doctoral thesis of Kamen [8] following the works of [63–65]. It is a thermo-mechanical testing setup situated inside a temperature controlled room and used to conduct mechanical measurements and tests on cementitious specimens, from a very early age directly after casting, at different temperatures. Quasi–isotherm temperature conditions were ensured in the specimen with the help of a cooling circuit surrounding the molds. A schematic diagram of the TSTM setup is shown in Fig. 2.

The setup consists of two devices; the Free Setup (FS) helps to measure the free autogenous deformations. The Restrained Setup (RS) helps in measuring the eigenstresses developing under various restraint conditions with the help of a load cell and controlling their development with an electromechanical actuator linked to a closed loop control system. The associated free deformations in the restrained specimen as well as the free deformations in the free system were measured by means of two LVDT in each specimen, attached to a rod inserted in the material, immediately after casting. In the RS setup, two LVDT namely LVDT A and LVDT B with an accuracy range of ±0.5 mm were placed

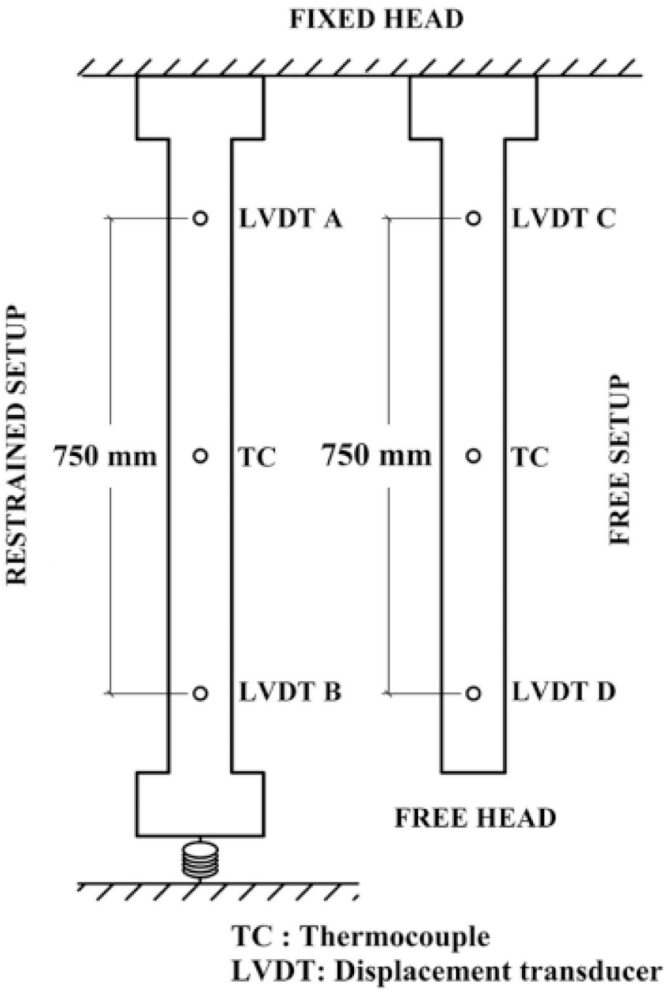

Fig. 2. Schematic representation of the TSTM setup. (Adapted after [8,21].)

750 mm apart, whereas in the FS setup, two LVDT namely LVDT C and LVDT D with an accuracy range of ±2.5 mm were installed 750 mm apart from each other, as shown in Fig. 2. The eigenstresses were calculated by dividing the force measured by the load cell of the RS setup with the cross sectional area of the specimen. In both devices, fully sealed specimens of cross sectional dimensions 50 mm × 100 mm were used. Further details regarding the TSTM setup can be found in [8,9,21,55].

2.5. Loading programs for the TSTM tests

Two types of tests were conducted in the TSTM; full restraint tests and partial restraint tests, both at a quasi-isothermal temperature of 20 °C. All measurements were started immediately after casting.

In the full restraint test, the specimen was subjected to fully restrained conditions against any autogenous or thermal deformations, from the time of casting, until a month or more. In order to carry this out, an active control was required to keep at zero the relative displacement between two points A and B 750 mm apart. However, at fresh state and in the very early age close to setting time, the material stiffness was too low to impose a closed loop force or deformation control. As such, the tests were started under stroke control (passive control) with the stroke remaining at the same position as the start of the test. The monitored development of eigenstresses under passive stroke control was used to determine a trigger value to activate the deformation control leading to full restraint condition. A value of 0.2 MPa (corresponding to a force of 100 kg carried by the specimen) was chosen as the trigger value, to be low enough to minimize the discrepancies of the control mode and the impacts on the viscous effects of the loading history, while being high enough to reach a sufficient stiffness of the specimen to respond to a closed loop deformation control without yielding out of control.

After the setting of the UHPFRC, when the stress in the material reached 0.2 MPa, the control was automatically switched to deformation control, wherein the relative displacement between the points A and B was kept zero. The control was therefore an active control as the deformations were controlled actively depending on the autogenous deformations occurring in the material, thereby ensuring full restraint conditions in the material.

In the partial restraint test, the entire test was controlled using stroke control and the stroke was kept in the same relative position without any movement, from the beginning of the test until the end. Because of the finite stiffness of the machine parts, due to which there were slight displacements of the machine parts, the specimen was not fully restrained in this case. The partial restraint imposed by the machine in these tests were calculated to be 54% in the Mix I-20C-PR1 test and 60% in the Mix I-20C-PR2, by comparing the free deformations in the restrained system and the free deformations in the free system. It can then be assumed that the stroke controlled test impose a restraint of about 50–60%.

The temperature evolution in the restrained and free specimens was monitored using thermocouples inserted into the specimens right after casting. No active temperature control was used. The temperature of the samples increased slightly (1 °C–2.2 °C) due to the heat of hydration, even though the molds contained cooling circuits to maintain the temperature. As such, the tests could not be considered to be fully under isothermal conditions but were under quasi-isothermal conditions.

It was assumed that the autogenous deformation varies linearly from one end to the other in the FS setup. The autogenous shrinkage was calculated by dividing the difference of displacements shown by LVDT C and D by the distance between them, that is, 750 mm. It was assumed that for each test, the restrained specimens exhibited similar autogenous shrinkage as that in the free specimens. For the Mix I, two full restraint tests (Mix I-20C-FR1, Mix I-20C-FR2) and two partial restraint tests (Mix I-20C-PR1, Mix I-20C-PR2) were carried out, whereas for the Mix II, only two full restraint tests were conducted (Mix II-20C-FR1, Mix II-20C-FR2).

3. Results and discussion

3.1. Development of dynamic elastic modulus

The development of the dynamic modulus of elasticity is shown in Fig. 3 on a semi-log scale. The static elastic moduli determined from compression test, after SIA 262/1-Annex G, on 70 mm × 140 mm cylinders are also shown in Fig. 3 for Mix 1 (7 days) and Mix II (7, 14, 28 days). As expected, the dynamic elastic moduli of the mixes are slightly higher than the static ones. The dynamic elastic modulus of Mix I stabilized around 52 GPa for specimen C1 and about 50 GPa for specimen C2, whereas that of Mix II reached about 50 GPa after 200 h.

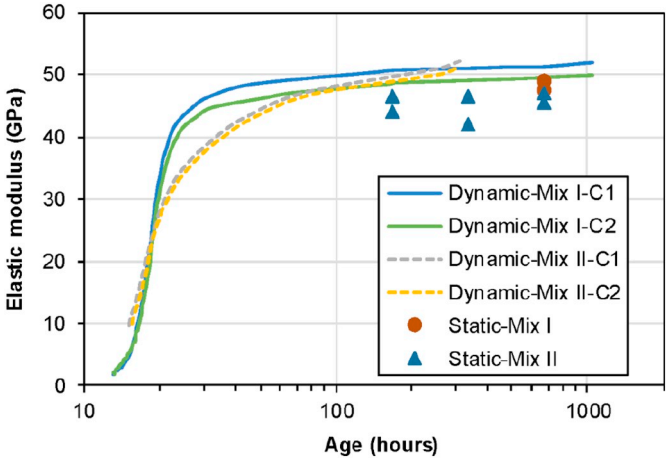

Fig. 3. Development of dynamic elastic moduli of Mix I and II obtained from the VRF tests. The static modulus of elasticity of both the mixes is also shown at 7, 14 and 28 days.

The main difference in the development of the dynamic modulus in the mixes occurs around 20 h as can be seen from Fig. 3. At this time, the rate of development of the dynamic elastic modulus becomes much lower in the case of Mix II when compared to that of Mix I. However, at a later age, the trend inverts and the rate of development of the dynamic elastic modulus of Mix I becomes lower than that of Mix II. Eventually the dynamic elastic moduli reach similar values at an age of about 200 h.

This trend could be explained by the difference in the two main parameters; the silica fume/cement (SF/C) ratio and the water/cement (W/C) ratio. Mix I has a SF/C ratio of 0.26 and Mix II has a SF/C ratio of 0.4, whereas the W/C ratio of Mix I is 0.163 and that of Mix II is 0.310. Jensen [33] has shown the influence of SF/C ratio and the W/C ratio on the rate of drop of relative humidity in cement paste specimens. The kinetics of the changes in the relative humidity is closely related to the kinetics of the rate of hydration in different mixes. As such, even though the relative humidity changes with age were not studied for the mixes in the present study, the expected trends of the same might indicate possible explanations for the kinetics of rate of development of dynamic elastic modulus. According to Jensen [33], as shown in Fig. 4, an increase in the SF/C ratio leads to an increase in the rate of drop of relative humidity in cement paste specimens in the early age and consequently an increase in the rate of overall hydration in the specimens. However, [32] has shown that only 20% mass of the silica fume contributes to the pozzolanic reaction, as all the $Ca(OH)_2$ will be consumed and the pozzolanic reaction gets saturated. Since the SF/C ratio for both mixes is higher than 0.2, it can be assumed that it has minimal effect on the trend of hydration. On the other hand, Fig. 4 also shows a similar trend of increase in the rate of drop of relative humidity with a decrease in the W/C ratio [33]. Hence, the reduced rate of development of dynamic elastic modulus for Mix II in the early age can be attributed predominantly to the dilution effect (effect of higher W/C ratio). Fig. 4 shows that the relative humidity drop is much faster as the W/C ratio decreases, but ultimately becomes similar for W/C ratio less than or equal to 0.3. The trend is similar to that of the dynamic elastic modulus in Fig. 3, in which the development is faster in Mix I with lower W/C ratio, but ultimately becomes similar in both mixes at a later age. Similar trends were also observed in [66,67] in ternary cement binders with SCM.

3.2. Heat of hydration

The heat of hydration of both the matrices (without fibers) was obtained from the isothermal calorimetry tests. Fig. 5 shows the heat flow per unit volume of both mixes. Four measurements are shown for

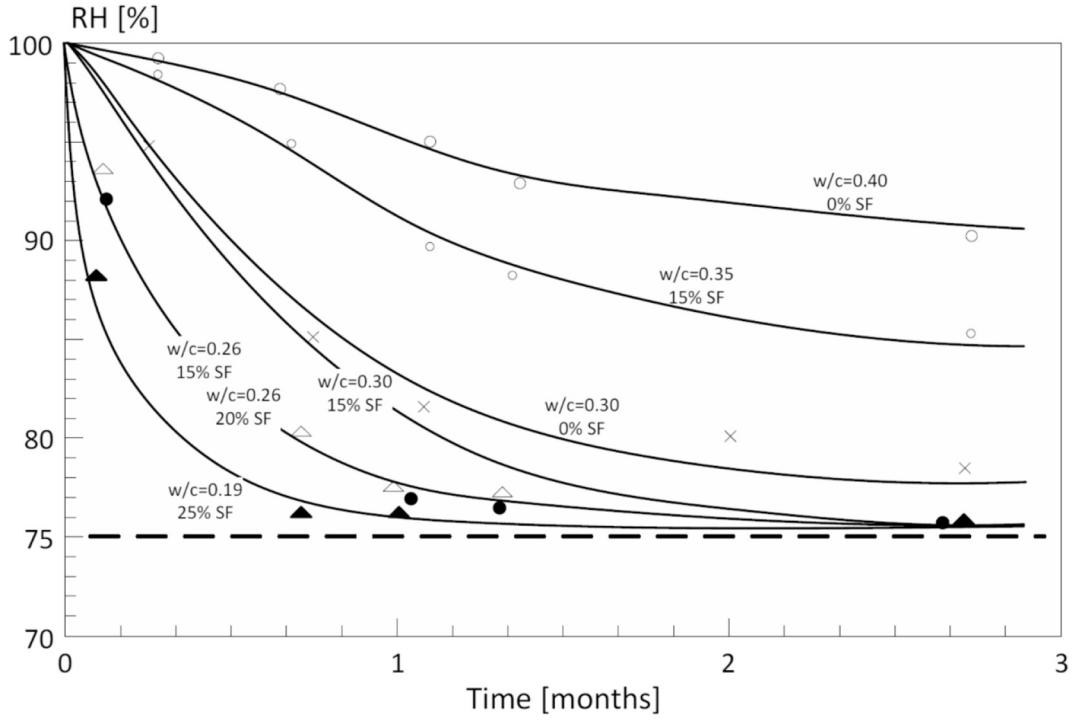

Fig. 4. Figure showing the effect of silica fume content and the water/cement ratio on the relative humidity within various cement paste and mortar specimens. (Taken from [33].)

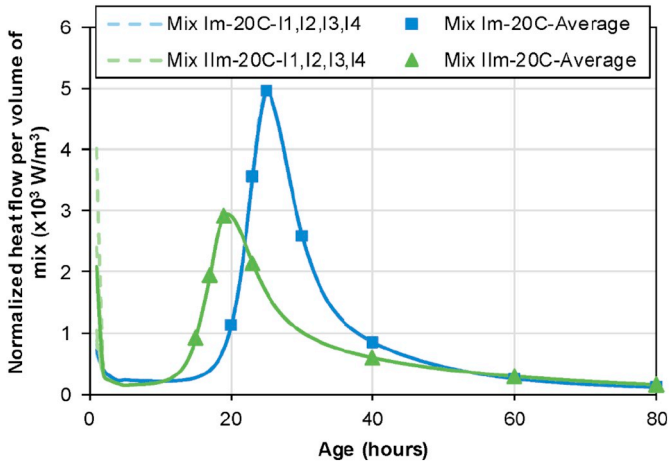

Fig. 5. Heat flow per unit volume of Mix I_m and Mix II_m, from isothermal calorimetry tests at 20 °C.

each mix. However, the scatter between the four tests was very low and therefore the curves were almost superimposed on each other. The volume of the 10 g of paste put in the ampoule was calculated using the specific weight of both the mixes (2295.9 kg/m^3 for Mix I_m and 2199.6 kg/m^3 for Mix II_m). Fig. 5 shows a higher dormant period for Mix I_m, which is due to the higher amount of superplasticizer needed to reach the minimum workability. Fig. 6a shows that the cumulative heat per unit volume of the Mix II_m is lower than that of Mix I_m, which could be explained by the limited reactivity of the limestone filler particles in Mix II_m and also due to the dilution effect in the same. Even though the limestone filler acts as nucleation sites for the hydration of more cement, the dilution effect dominates the nucleation effect and thereby releases less heat in the early age. Similar trends were seen in the case of blended cements in [66,68,69]. In the case of UHPC mixes, it was shown in [70] that the cumulative heat per unit volume of binder were almost similar up to 54% replacement of cement with limestone filler, whereas it was much lesser when the limestone filler replacement reached 74%.

The cumulative heat released can be used to calculate the degree of hydration of the mixes. Table 5 shows the hypothetical value of the total potential heat release for both the mixes, at full hydration, assuming that only cement and silica fume contributes to the release of heat. Based on literature data [9,32], it was also assumed that only 20% mass of the silica fume will contribute to the heat of hydration, as all the $Ca(OH)_2$ will be consumed by then and there will not be any more pozzolanic reaction, that is, maximum mass of silica fume reacting is equal to 20% of the mass of the cement. Fig. 6b shows the degree of hydration curves for both the mixes, which was obtained by dividing the cumulative heat per unit volume of the mixes (obtained from the isothermal calorimetry tests) by the total potential heat of the respective mix, $Ht_{100\%}$ at full hydration, as seen in Table 5. Fig. 6b shows that the degree of hydration of Mix II_m at 650 h is about 49.5% whereas that of Mix I_m at 650 h is only 28.7%.

3.3. Temperature evolution in the TSTM

Fig. 7 shows the evolution of the temperature in the restrained specimens in the TSTM. The main observations in the evolution of the temperature are summarized in Table 6, which shows that the rise in the temperature in Mix I is higher (1.8 °C–2.2 °C) than in Mix II (1.0 °C). Since the rise in the temperature in the specimens is small (max of only 2.2 °C), the test can be considered as a quasi-isothermal test.

As discussed later in Section 3.4, the eigenstresses start developing at the end of the apparent swelling and therefore the end of apparent swelling could be considered as an apparent setting time. Fig. 7 shows the corresponding points on the temperature curves, which is also summarized in the Table 6. It can be seen that the apparent setting time occurs when the rise in temperature is approximately 27%–41.5% of the total rise in temperature in the specimen. The corresponding eigenstresses at these points are also less than or equal to 0.06 MPa, except for Mix I-20C-PR1 where the stress was 0.12 MPa. These values of eigenstresses are very low and therefore the end of apparent swelling

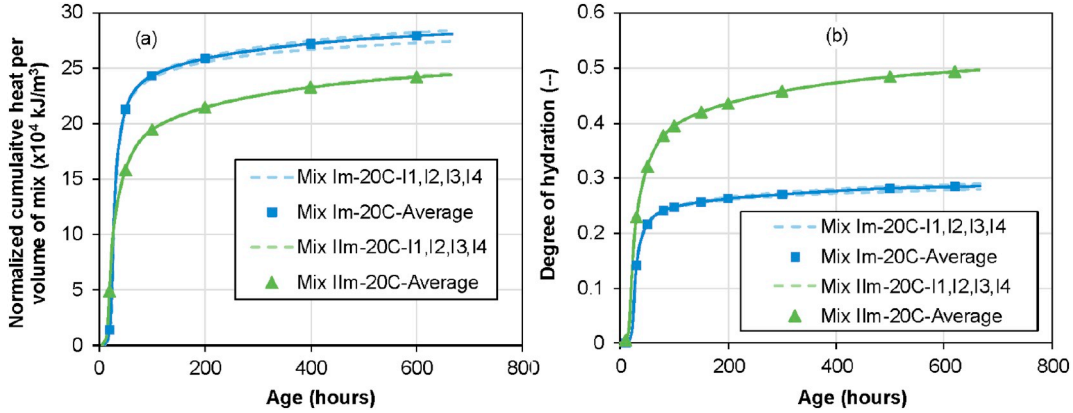

Fig. 6. a) Cumulative heat per unit volume of Mix I_m and Mix II_m, from isothermal calorimetry tests at 20 °C, b) overall degree of hydration of Mix I_m and Mix II_m at 20 °C.

Table 5
Total potential heat release of Mix I and II at full hydration, $Ht_{100\%}$.

Mix	Cement reacted (kg/m^3)	Heat release of cement (kJ/kg)	Silica fume reacted (kg/m^3)	Heat release of silica fume (kJ/kg)[32]	Total potential heat at full hydration, $Ht_{100\%}$ (kJ/m^3)
Mix I	1607.9	452.3	321.6	780	978,085
Mix II	809.6	452.3	161.9	780	492,480

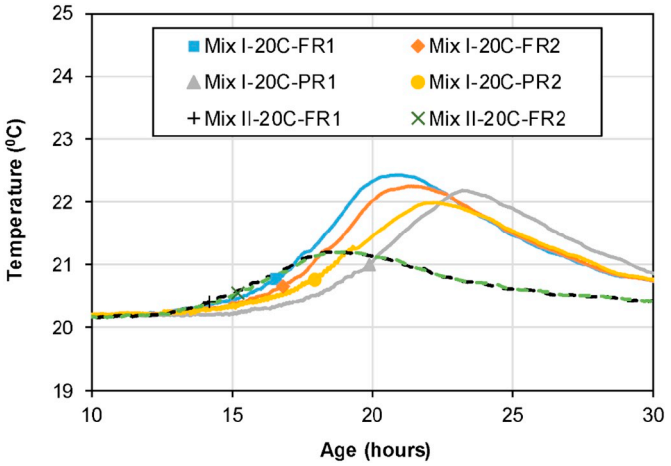

Fig. 7. Evolution of temperature in the restrained test specimens in the TSTM setup (focusing near the peak of the temperature curves).

Table 6
Trends of temperature evolution in the TSTM experiments.

Experiment	ΔT_{tot}^* (^0C)	t_{peak}^* (hours)	t_{as}^* (hours)	ΔT_{as}^* (^0C)	$\Delta T_{as}/\Delta T_{tot}^*$ (%)	σ_{as}^* (MPa)
Mix I–20C-FR1	2.2	20.9	16.6	0.66	30.0	0.06
Mix I-20C-FR2	2.0	21.3	16.8	0.54	27.0	0.04
Mix I-20C-PR1	2.0	23.2	19.9	0.83	41.5	0.12
Mix I-20C-PR2	1.8	22.2	17.9	0.55	30.6	0.04
Mix II-20C-FR1	1.0	18.3	14.2	0.28	28.0	0.01
Mix II-20C-FR2	1.0	18.9	15.2	0.41	41.0	0.06

* ΔT_{tot}: total rise in temperature, t_{peak}: time to peak of the temperature curve, t_{as}: time to the end of apparent swelling of autogenous deformations (apparent setting time), ΔT_{as}: rise in temperature up to the end of apparent setting time, σ_{as}: eigenstress value at the apparent setting time.

can be considered as the apparent setting time in the mixes.

3.4. Development of autogenous deformations

The free autogenous deformations $\varepsilon_{free}^{free}$ were measured using the FS setup of the TSTM and the autogenous shrinkage was calculated as explained in Section 2.5. Figs. 8, 9 and 10 show the development of $\varepsilon_{free}^{free}$ corresponding to the different tests. Fig. 8 shows the development of autogenous deformations as measured, whereas Fig. 9 shows the evolution of autogenous deformations zeroed at the end of swelling. Fig. 10 compares the kinetics of the autogenous deformation curves for each mix and defines the different phases in their evolution.

In Fig. 10, Point A is the time of contact of water with the binders and it is considered as the "zero age" of the material. Point B is the point where the test measurements start. The phase AB is the phase in which the mixing procedure as well as the casting of the mix into the molds take place. It can be seen that there is a swelling phase in all the mixes (phase BC). The point C is the end of the apparent swelling phase of the material, after which the actual shrinkage deformations begin, which lead to the development of eigenstresses in the material. The point C is in the range of 16.5–19.5 h in the case of Mix I whereas it is in the range of 14.5–15.5 h for Mix II.

Point D is the point that shows a major difference in the two mixes. While for Mix I, even though there is a reduction in the rate of shrinkage deformations beyond the point D, the shrinkage deformations are still increasing and there is no reduction (or swelling) in the value of the same; whereas for Mix II, a clear reduction in the autogenous deformations (shoulder effect) can be observed at the point D. Jensen [33] showed a similar trend in the reduction of the relative humidity in cementitious materials with silica fume. Kazemi Kamyab [9] also showed a similar trend using Proton NMR (^{1}H NMR). It is assumed that it is around the point D, that the silica fume starts to react which could lead to a change in the rate of hydration, which in turn leads to a change in the rate of autogenous shrinkage occurring in the material. Point E is the point where the temporary swelling ends for the Mix II whereas for Mix I, it is the point where the rate of development of autogenous deformations changes slightly. The phase EF is similar in both the mixes, even though there may be slight differences in the rate of development of the autogenous deformations.

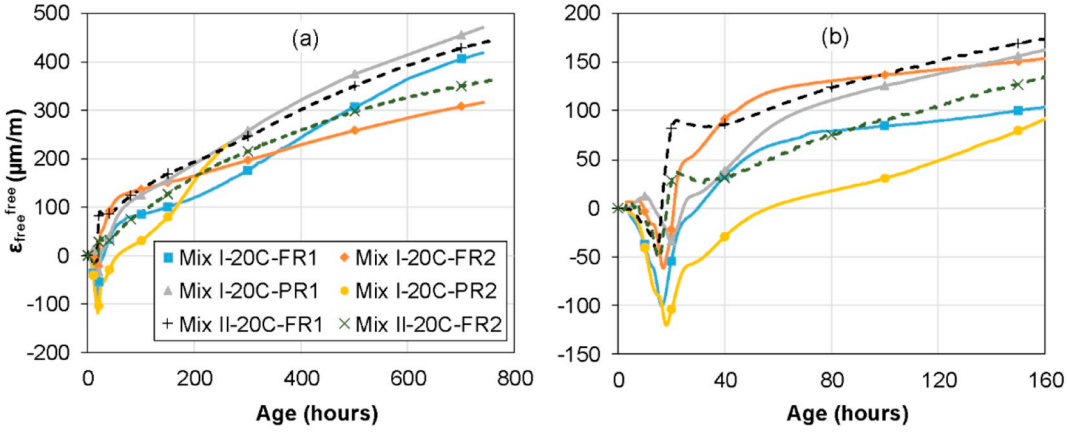

Fig. 8. Evolution of free autogenous deformations (increasing deformation represents shrinkage) in the FS setup of the TSTM; a) overall trend, b) early age.

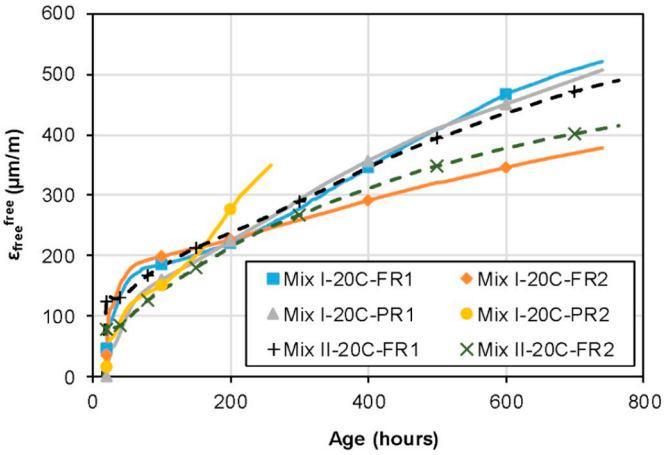

Fig. 9. Evolution of autogenous deformations zeroed at the end of the swelling phase.

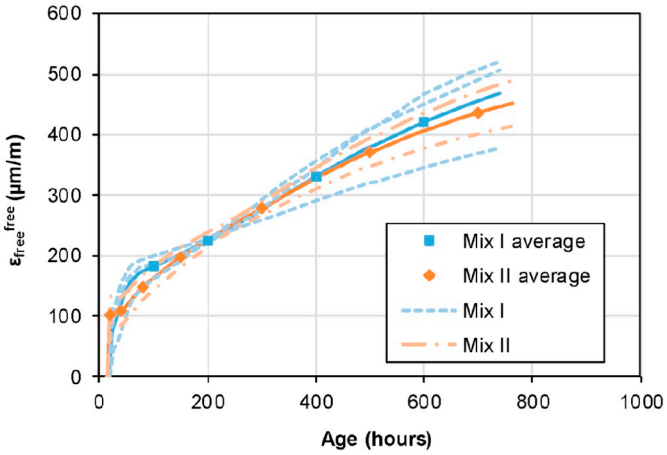

Fig. 11. Average shrinkage curves of Mix I and Mix II from the FS setup of the TSTM.

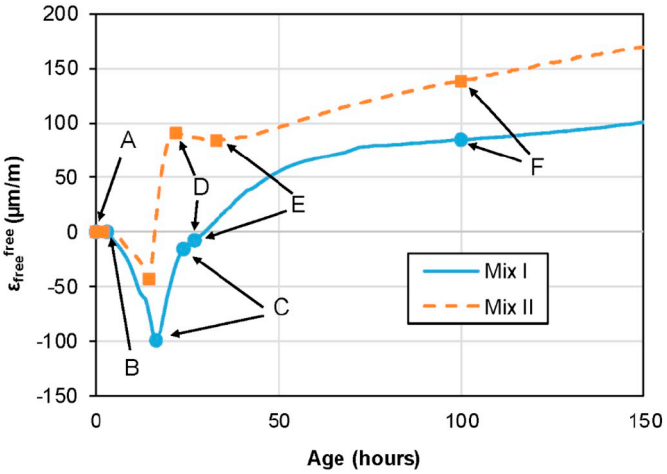

Fig. 10. The different phases in the evolution of the autogenous deformations of Mix I and II, in the FS setup of the TSTM.

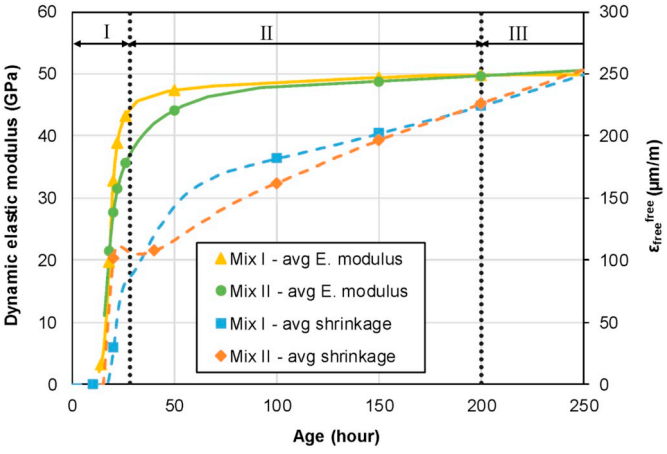

Fig. 12. Comparison of the evolution of the autogenous shrinkage in Mix I and II with the corresponding development of elastic modulus.

Another interesting observation, as shown in Figs. 11 and 12, is the comparison of the average autogenous shrinkage curves for the two mixes along with their corresponding development of dynamic elastic modulus. The autogenous shrinkage of Mix II shows a reduction around 20–22 h and it is approximately around this time that the rate of development of dynamic elastic modulus of Mix II deviates from that of Mix I, marked as zone II in Fig. 12. It can also be seen that the autogenous shrinkage curves of both mixes become almost similar approximately at the same time when the average dynamic elastic modulus of both mixes become similar (zone III in Fig. 12).

This trend can be explained using the capillary pressure hypothesis [16,71–73], which states that the capillary tension (or depression) in the liquid phase in the pores, exerts a pressure on the solid skeleton (hydrates) formed, which then undergoes a compression and therefore a shrinkage (autogenous). However, the elastic stiffness and the viscous

response of the solid skeleton of the matrix help in mitigating the effect of the capillary tension. As the hydration progresses, the pore structure becomes finer, which in turn leads to a higher capillary tension and thereby a higher autogenous shrinkage. The hydration also leads to the consumption of the water in the pores, which is another reason for the increase in the capillary tension in the liquid phase. In zone II in Fig. 12, the dynamic elastic modulus of Mix II is slightly lesser than that of Mix I. It can then reasonably be assumed that the pore structure in Mix II will be coarser than the same for Mix I in this zone. As a coarser pore structure leads to a lesser value of capillary stress, the autogenous shrinkage produced will also be lesser. This might be the possible explanation for the slightly lower autogenous shrinkage for Mix II in zone II when compared to Mix I. It also explains why the average autogenous shrinkage values of both mixes become similar when the average dynamic elastic moduli become similar in the zone III.

Fig. 8a shows that the long term autogenous shrinkage varies between 376 μm/m and 514 μm/m at 720 h (one month) for Mix I whereas that for Mix II varies between 405 μm/m and 477 μm/m. At an age of 7 days at 20 °C, Kamen [8] reported an autogenous shrinkage, which varied between 105 μm/m and 140 μm/m for a UHPFRC mix similar to Mix I, whereas Switek [21] reported an autogenous shrinkage of 168 μm/m at 7 days. The results in the present study exhibit slightly higher values for the autogenous shrinkage at 7 days with Mix I showing a value ranging from 202 μm/m to 225 μm/m and Mix II from 193 μm/m to 222 μm/m. The slightly higher values can be explained by the changes in the dormant period of the mixes in the present study when compared to that of [8,21]. The Mix I in the present study have an approximate dormant period of 11 h whereas the dormant period of the mixes used in [8,21] varied between 32 and 33 and 22 and 24 h respectively. This is mainly because of the variation in the amount of superplasticizer used in the mixes. The Mix I in the present study has a superplasticizer dosage of 1.4% whereas that in [21] was 2.3% and in [8] was 3.3%. As such, the present mixes have slightly higher autogenous shrinkage at 7 days.

3.5. Development of eigenstresses

Fig. 13a shows the displacements of LVDT A and B from the Mix I-20C-FR1 test. It can be seen that both are exact mirror images of each other, ensuring zero relative displacement between the two, thereby ensuring full restrained conditions. Fig. 13b shows the displacements of LVDT A and B from the Mix I-20C-PR1 test and unlike that in the full restraint test, the displacements are not mirror images of each other and thereby the relative displacement between them is non zero and therefore the restraint imposed is only partial.

At this point, it is interesting to compare the procedure for full restraint adopted in the present study, with another commonly used procedure in literature. Following the procedure developed by [74], [2,34,75] had conducted full restraint tests on UHPFRC mixes similar to Mix I in the present study in similar TSTM setups, to study the development of eigenstresses. The procedure was to allow the specimen to shrink from its initial position up to 5-6 μm and then to bring the specimen back to its initial zero position, which induced stresses in the material. The cycle was then repeated again for every 5–6 μm increments. Fig. 14a compares the development of eigenstresses using this procedure with that adopted in the present study using deformation control and it can be seen that the stresses at any given age are slightly lesser in the case of the incremental procedure, when compared to that of Mix I. Fig. 14b depicts the development of eigenstresses with the age axis of the mixes in [2,34] adjusted in such a way so that the stresses start to develop at the same age as that of the Mix I. But even then it can be seen that the stresses are developing much faster in the experiments in the present study, which shows that the incremental procedure adopted in [2,34] does not guarantee full restraint. However, it should be noted that the difference in the values of eigenstresses between the different procedures is not that large and may be even attributed to the slight difference in the composition of the mixes tested. Nevertheless, the procedure developed in the present study is much easier to carry out and also easier to model. On the other hand, the incremental procedure helps in the determination of local estimate of the elastic modulus during the incremental loading steps as the elastic strain and stress could be measured at these loading steps.

Fig. 15 shows the development of eigenstresses in the two mixes under the different restraint conditions. As expected, the eigenstresses developed in the case of full restraint tests were much higher than that in the partial restraint tests for Mix I. The stresses reached a value of 12.2 MPa and 11.7 MPa at an age of one month (720 h) in the two full restraint tests for Mix I, whereas the stresses were only about 5.3 MPa in the partial restraint tests for the same age. The rate of development of eigenstresses under full restraint were much slower for Mix II, with the values being only 6.9 MPa and 5.4 MPa for Mix II-20C-FR1 and Mix II-20C-FR2 respectively, at an age of one month. However, the eigenstresses kept on developing even beyond one month, with Mix I-20C-FR2 reaching a stress value above 14 MPa (in the strain hardening domain) at around 1900 h (2.6 months) and Mix II-20C-FR2 reaching a stress value of 12.3 MPa (just below the strain hardening domain) at around 2400 h (3.3 months). It indicates that even though the rate of eigenstresses development is slower for Mix II, the eigenstresses can still reach values close to the strain hardening domain at a later age.

The lower value of eigenstresses might be explained by a higher viscoelastic response of Mix II, and consequently a higher relaxation potential, which will help in relaxing the developed eigenstresses. This was confirmed by conducting tensile creep tests for both mixes on prismatic specimens of dimensions 1000 mm × 70 mm × 40 mm, at

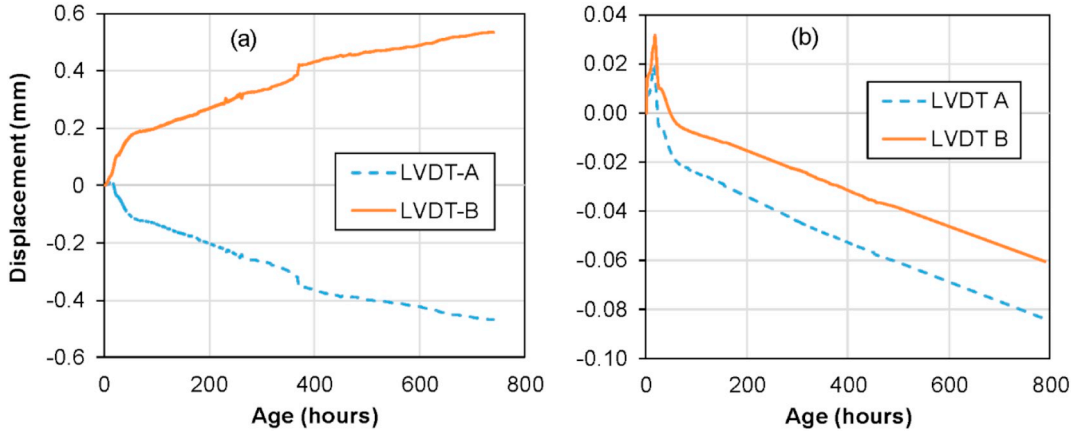

Fig. 13. Comparison of LVDTs A and B in the; a) Mix I-20C-FR1 full restraint test, b) Mix I-20C-PR1 partial restraint test.

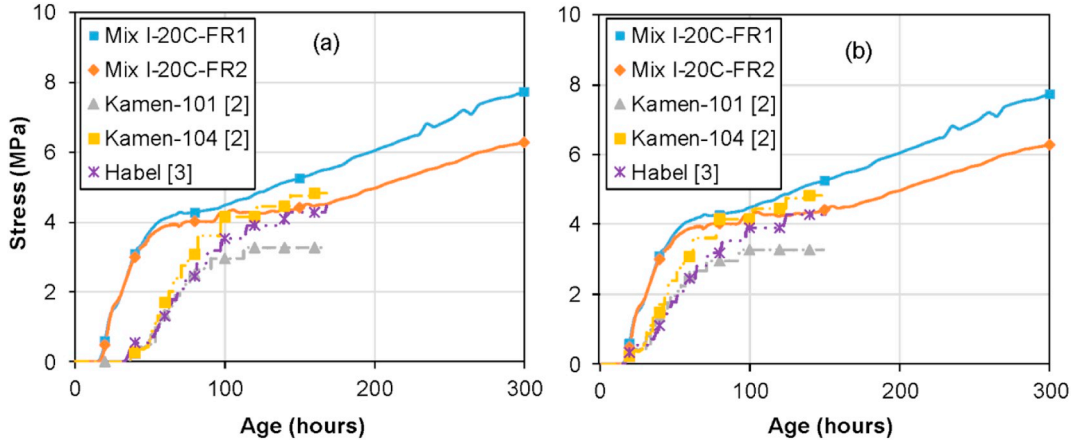

Fig. 14. Comparison of the development of eigenstresses in the full restraint tests in the present study and tests using the incremental procedure of [2,3]; a) time scale as measured, b) time scale adjusted.

different stress levels. The details regarding the tensile creep rigs and the test setup can be found in [21,30]. Fig. 16 shows the average normalized specific creep curves for both mixes under tension, loaded at an age of 14 days, at different stress levels. Mix II exhibits a higher creep response throughout the period of loading, thereby confirming a much higher viscous response, and consequently a higher relaxation potential.

The reduced eigenstresses in Mix II may also be due to slower rate of development of elastic modulus in Mix II, as discussed in Section 3.1. A combination of slightly lower elastic modulus as well as lower autogenous shrinkage may have led to a slower development of eigenstresses. The drop in the autogenous shrinkage (point D in Fig. 10) has also led to a decrease in the eigenstresses in Mix II, as can be seen clearly from Fig. 15b, whereas a similar drop in autogenous shrinkage and a consequent reduction in eigenstresses were not present in the case of Mix I. Bouasker et al. [66] and Mehdipour et al. [67] observed similar trends in ternary cement binders with limestone filler and reported that the time to cracking was much higher in the case of ternary binders with limestone fillers, when compared to cement binders without limestone filler. As such, the tests show that it is advantageous to use the mix with limestone filler, as the adverse effects of the eigenstresses as well as the cracking risk are considerably reduced.

Fracture tests were later conducted on all the specimens and the tensile strengths are summarized in Table 7. The tensile strength results were consistent with the values shown in [21], who obtained an average tensile strength of 15.5 MPa for specimens of similar dimensions loaded at 10 days for a similar mix. Uniaxial tensile tests were also conducted on dumbbell specimens of Mix I and Mix II, with cross

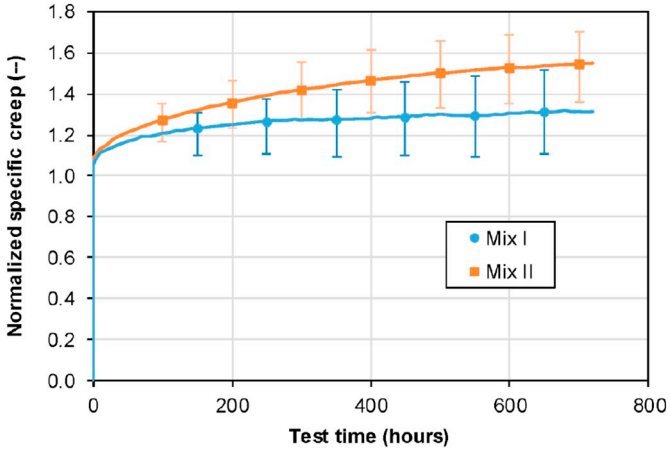

Fig. 16. Average normalized specific creep of Mix I and II under tension, loaded at an age of 14 days.

sections of 50 mm × 30 mm, in an electromechanical test setup at very low strain rates of 10^{-8} 1/s. The tests showed average elastic limits of 9.60 MPa and 10.19 MPa and average tensile strengths of 15.79 MPa and 17.17 MPa respectively for Mix I and Mix II at an age of 14 days age.

Table 7 shows that the eigenstresses at 720 h in the full restraint tests on Mix I, were much higher than the other tests and even higher than the elastic limit of the material. As such, the stress levels had

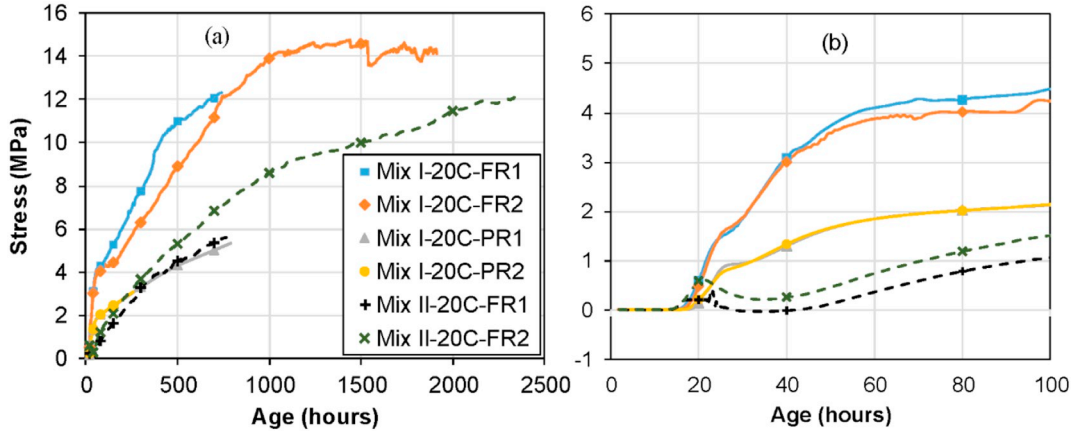

Fig. 15. Development of eigenstresses in the full and partial restraint tests in the RS setup of the TSTM; a) overall trend, b) early age behavior.

Table 7
Summary of fracture tests done in the TSTM.

Specimen	Eigenstresses at 720 hours (MPa)	Tensile strength (MPa)	Eigenstresses as a percent of tensile strength after 720 hours (%)
Mix I-20C-FR1	12.23	12.8	95.54
Mix I-20C-FR2	11.71	16.6	70.54
Mix I-20C-PR1	5.07	18.18	27.89
Mix I-20C-PR2	–	17.02	–
Mix II-20C-FR1	5.42	16.02	33.83
Mix II-20C-FR2	6.93	17.38	39.87

clearly reached the strain hardening domain of the tensile response of the material. On the other hand, the eigenstresses development was much slower in the Mix II, with the values of the eigenstresses after 720 h being only about 33–40% of the tensile strength of the mix and also below the elastic limit. This clearly confirms the advantage of the limestone filler mix in terms of the cracking risk and serviceability.

4. Conclusions

- Tests on UHPFRC under full restraint conditions were done for the first time and they showed that the eigenstresses could reach values higher than the elastic limit and even close to the ultimate strength of the material.
- A new closed loop deformation controlled method was proposed to carry out tests under full restraint conditions. A value of 0.2 MPa was chosen as the trigger value to activate the closed loop of deformation control, to be low enough to minimize the discrepancies of the control mode and the impacts on the viscous effects of the loading history, while being high enough to demonstrate a sufficient stiffness of the specimen to respond to a closed loop deformation control without yielding out of control.
- Two mixes were investigated; Mix I with pure type I cement and silica fume and Mix II with silica fume and 50% replacement of type I cement with limestone filler.
- The development of the elastic modulus and autogenous shrinkage were almost similar in both Mix I and Mix II, except for changes in the kinetics at certain ages.
- Isothermal calorimetry tests were conducted which showed that the degree of hydration of Mix II at 650 h is about 49.5% whereas that of Mix I at 650 h is only 28.7%.
- The rate of development of eigenstresses under full restraint conditions were much slower in Mix II when compared to Mix I, with Mix I reaching the strain hardening domain at around 720 h (one month), whereas for Mix II the eigenstresses were only approaching the strain hardening domain, even after 3 months. However, the results indicated that even for Mix II, the eigenstresses might reach the strain hardening domain at a later age beyond 3 months.
- This study highlighted the necessity of using a strain hardening material for casting UHPFRC on an existing substrate, in order to avoid localized macrocracking and meet the serviceability criteria associated to the protective function.

Declaration of Competing Interest

The authors declare that they have no known competing financial interests or personal relationships that could have appeared to influence the work reported in this paper.

Acknowledgements

The project was financially supported by the Swiss National Science Foundation (grant 200021_153394/1). The authors would like to appreciate the help given by the technicians of GIC-ENAC-EPFL in performing the experimental works with the TSTM.

References

[1] E. Denarié, E. Brühwiler, Cast-on Site UHPFRC for improvement of existing structures – achievements over the last 10 years in practice and research, High Perform. Fiber Reinf. Cem. Compos, vol. 7, 2015, pp. 473–480.
[2] A. Kamen, E. Denarié, H. Sadouki, E. Brühwiler, Thermo-mechanical response of UHPFRC at early age - experimental study and numerical simulation, Cem. Concr. Res. 38 (2008) 822–831, https://doi.org/10.1016/J.CEMCONRES.2008.01.009.
[3] K. Habel, Structural Behaviour of Elements Combining Ultra-high Performance Fibre Reinforced Concretes (UHPFRC) and Reinforced Concrete, Doctoral thesis No: 3036 Ecole Polytechnique Fédérale de Lausanne, Switzerland, 2004.
[4] K. Habel, J.P. Charron, E. Denarié, E. Brühwiler, Autogenous deformations and viscoelasticity of UHPFRC in structures. Part I: experimental results, Mag. Concr. Res. 58 (2006) 135–145.
[5] E. Denarié, J. Silfwerbrand, H. Beushausen, Structural behaviour, Bond. Cem. Mater. Overlays Repair, Lining or Strength. Slabs or Pavements, Springer, 2011, pp. 81–106.
[6] P. Schiessl, K. Beckhaus, I. Schachinger, P. Rucker, New results on early-age cracking risk of special concrete, Cem. Concr. Aggregates. 26 (2004) 1–9.
[7] I. Schachinger, K. Schmidt, D. Heinz, P. Schießl, Early-age cracking risk and relaxation by restrained autogenous deformation of ultra high performance concrete, 6th Int. Symp. High Strength/High Perform. Concr., Leipzig, Germany, 2002, pp. 1341–1354.
[8] A. Kamen, Comportement au jeune âge et différé d'un BFUP écrouissant sous les effets thermomécaniques, Doctoral thesis No: 3827 Ecole Polytechnique Fédérale de Lausanne, Switzerland, 2007.
[9] M. Kazemi Kamyab, Autogenous Shrinkage and Hydration Kinetics of SH-UHPFRC Under Moderate to Low Temperature Curing Conditions, Doctoral Thesis No: 5681, Ecole Polytechnique Fédérale de Lausanne, Switzerland, 2013.
[10] D.-Y. Yoo, J.-J. Park, S.-W. Kim, Y.-S. Yoon, Influence of ring size on the restrained shrinkage behavior of ultra high performance fiber reinforced concrete, Mater. Struct. 47 (2014) 1161–1174, https://doi.org/10.1617/s11527-013-0119-0.
[11] D.-Y. Yoo, N. Banthia, Y.-S. Yoon, Geometrical and boundary condition effects on restrained shrinkage behavior of UHPFRC slabs, KSCE J. Civ. Eng. 22 (2018) 185–195, https://doi.org/10.1007/s12205-017-0587-9.
[12] A.M. Soliman, M.L. Nehdi, Effect of partially hydrated cementitious materials and superabsorbent polymer on early-age shrinkage of UHPC, Constr. Build. Mater. 41 (2013) 270–275, https://doi.org/10.1016/J.CONBUILDMAT.2012.12.008.
[13] J. Liu, Z. Ou, J. Mo, Y. Chen, T. Guo, W. Deng, Effectiveness of saturated coral aggregate and shrinkage reducing admixture on the autogenous shrinkage of ultrahigh performance concrete, Adv. Mater. Sci. Eng. 2017 (2017) 1–11.
[14] A. Kamen, E. Denarié, H. Sadouki, E. Brühwiler, UHPFRC tensile creep at early age, Mater. Struct. 42 (2008) 113–122, https://doi.org/10.1617/s11527-008-9371-0.
[15] P. Rossi, J.P. Charron, M. Bastien-Masse, J.L. Tailhan, F. Le Maou, S. Ramanich, Tensile basic creep versus compressive basic creep at early ages: comparison between normal strength concrete and a very high strength fibre reinforced concrete, Mater. Struct. 47 (2014) 1773–1785.
[16] P. Acker, Swelling, shrinkage and creep: a mechanical approach to cement hydration, Mater. Struct. 37 (2004) 237–243, https://doi.org/10.1007/BF02480632.
[17] A. Loukili, P. Richard, J. Lamirault, A study on delayed deformations of an ultra high strength cementitious material, Spec. Publ. 179 (1998) 929–950.
[18] M. Cheyrezy, M. Behloul, Creep and shrinkage of ultra-high performance concrete, Creep, Shrinkage Durab. Mech. Concr. Other Quasi-Brittle Mater. (Concreep 6), 2001, pp. 527–538.
[19] V.Y.Y. Garas, K.E.E. Kurtis, L.F.F. Kahn, Creep of UHPC in tension and compression: effect of thermal treatment, Cem. Concr. Compos. 34 (2012) 493–502, https://doi.org/10.1016/J.CEMCONCOMP.2011.12.002.
[20] Y. Xu, J.J. Liu, J.J. Liu, P. Zhang, Q. Zhang, L. Jiang, Experimental studies and modeling of creep of UHPC, Constr. Build. Mater. 175 (2018) 643–652, https://doi.org/10.1016/J.CONBUILDMAT.2018.04.157.
[21] A.E. Switek, Time-dependent Response of Ultra High Performance Fibre Reinforced Concrete (UHPFRC) Under Low to High Tensile Stresses, Doctoral thesis No: 4899 Ecole Polytechnique Fédérale de Lausanne, Switzerland, 2011.
[22] V.Y. Garas, L.F. Kahn, K.E. Kurtis, Short-term tensile creep and shrinkage of ultra-high performance concrete, Cem. Concr. Compos. 31 (2009) 147–152, https://doi.org/10.1016/J.CEMCONCOMP.2009.01.002.
[23] V.Y. Garas, A.R. Jayapalan, L.F. Kahn, K.E. Kurtis, Micro- and nanoscale characterization of effect of interfacial transition zone on tensile creep of ultra-high-performance concrete, Transp. Res. Rec. 2141 (2010) 82–88, https://doi.org/10.3141/2141-14.

[24] P. Acker, M. Behloul, Ductal technology: a large spectrum of properties, a wide range of applications, Proc. Int. Symp. Ultra High Perform. Concr., Kassel, Germany, 2004, pp. 11–23.
[25] S.A. Altoubat, D.A. Lange, Tensile basic creep: measurements and behavior at early age, ACI Mater. J. 98 (2001) 386–393.
[26] D.S. Atrushi, Tensile and Compressive Creep of Early Age Concrete: Testing and Modelling, Doctoral thesis Norwegian University of Science and Technology, Norway, 2003.
[27] B. Bissonnette, D. Boily, J. Bastien, M. Fafard, Tensile creep of concrete repair materials: Recent experimental findings towards optimization, Creep, Shrinkage Durab. Mech. Concr. Other Quasi-Brittle Mater. (Concreep 6), 2001, pp. 599–604.
[28] S.A. Altoubat, D.A. Lange, Creep, shrinkage and cracking of restrained concrete at early age, ACI Mater. J. 98 (4) (2001) 323–331.
[29] A. Switek-Rey, E. Denarié, E. Brühwiler, Early age creep and relaxation of UHPFRC under low to high tensile stresses, Cem. Concr. Res. 83 (2016) 57–69.
[30] A. Switek-Rey, E. Denarié, E. Brühwiler, Tensile creep of UHPFRC under low and high stresses, 4th Int. Conf. Constr. Mater. – Performance, Innov. Struct. Implic., Nagoya, Japan, 2009, pp. 432–437.
[31] T.C. Powers, T.L. Brownyard, Studies of the physical properties of hardened portland cement paste, J. Proc. 43 (1946) 101–132, https://doi.org/10.14359/8745.
[32] V. Waller, Relations entre composition des bétons, exothermie en cours de prise et résistance à la compression, thèse de doctorat LCPC, Nantes, France, 2001.
[33] O.M. Jensen, Autogenous Phenomena in Cement-based Materials, Doctoral thesis Technical University of Denmark, 2005.
[34] K. Habel, P. Gauvreau, Response of ultra-high performance fiber reinforced concrete (UHPFRC) to impact and static loading, Cem. Concr. Compos. 30 (2008) 938–946, https://doi.org/10.1016/J.CEMCONCOMP.2008.09.001.
[35] P.L. Domone, S.M. N., Properties of high-strength concrete mixes containing PFA and GGBS, Mag. Concr. Res. 47 (1995) 355–367.
[36] S.J.J. Barnett, M.N.N. Soutsos, S.G.G. Millard, J.H.H. Bungey, Strength development of mortars containing ground granulated blast-furnace slag: effect of curing temperature and determination of apparent activation energies, Cem. Concr. Res. 36 (2006) 434–440 https://doi.org/10.1016/j.cemconres.2005.11.002.
[37] M. Nehdi, S. Mindess, P.-C. Aïtcin, Optimization of high strength limestone filler cement mortars, Cem. Concr. Res. 26 (1996) 883–893, https://doi.org/10.1016/0008-8846(96)00071-3.
[38] A. Tafraoui, G. Escadeillas, S. Lebaili, T. Vidal, Metakaolin in the formulation of UHPC, Constr. Build. Mater. 23 (2009) 669–674, https://doi.org/10.1016/J.CONBUILDMAT.2008.02.018.
[39] H. Yazıcı, H. Yiğiter, A.Ş. Karabulut, B. Baradan, Utilization of fly ash and ground granulated blast furnace slag as an alternative silica source in reactive powder concrete, Fuel 87 (2008) 2401–2407, https://doi.org/10.1016/J.FUEL.2008.03.005.
[40] Z. Wu, C. Shi, W. He, Comparative study on flexural properties of ultra-high performance concrete with supplementary cementitious materials under different curing regimes, Constr. Build. Mater. 136 (2017) 307–313, https://doi.org/10.1016/J.CONBUILDMAT.2017.01.052.
[41] Z. Jisong, Z. Yinghua, L. Haijiang, Experimental investigation and prediction of compressive strength of ultra-high performance concrete containing supplementary cementitious materials, Adv. Mater. Sci. Eng. 2017 (2017) 1–8.
[42] B.A. Gedam, N.M. Bhandari, A. Upadhyay, Influence of supplementary cementitious materials on shrinkage, creep, and durability of high-performance concrete, J. Mater. Civ. Eng. 28 (2016) 04015173(1-11), https://doi.org/10.1061/(ASCE)MT.1943-5533.0001462.
[43] R.D.D. Toledo Filho, E.A.B.A.B. Koenders, S. Formagini, E.M.R.M.R. Fairbairn, Performance assessment of Ultra High Performance Fiber Reinforced Cementitious Composites in view of sustainability, Mater. Des. 36 (2012) 880–888, https://doi.org/10.1016/j.matdes.2011.09.022.
[44] E. Denarié, Recommendations for the tailoring of UHPFRC recipes for rehabilitation, deliverable ARCHES D06, http://arches.fehrl.org, (2009).
[45] E. Denarié, E. Brühwiler, Strain hardening ultra-high performance fibre reinforced concrete: deformability versus strength optimization, Int. J. Restaur. Build. Monum. 17 (2011) 397–410.
[46] E. Ghafari, S.A. Ghahari, H. Costa, E. Júlio, A. Portugal, L. Durães, Effect of supplementary cementitious materials on autogenous shrinkage of ultra-high performance concrete, Constr. Build. Mater. 127 (2016) 43–48, https://doi.org/10.1016/J.CONBUILDMAT.2016.09.123.
[47] J. Liu, Z. Ou, J. Mo, Y. Wang, H. Wu, The effect of SCMs and SAP on the autogenous shrinkage and hydration process of RPC, Constr. Build. Mater. 155 (2017) 239–249, https://doi.org/10.1016/J.CONBUILDMAT.2017.08.061.
[48] C. Jiang, Y. Yang, Y. Wang, Y. Zhou, C. Ma, Autogenous shrinkage of high performance concrete containing mineral admixtures under different curing temperatures, Constr. Build. Mater. 61 (2014) 260–269 https://doi.org/10.1016/j.conbuildmat.2014.03.023.
[49] Y. Lyu, H. Huang, G. Ye, G. De Schutter, Autogenous shrinkage of low water-binder ratio cement pastes with supplementary cementitious materials, Fourth Int. Conf. Sustain. Constr. Mater. Technol, 2016, pp. 1–9.
[50] A.M.T. Hassan, S.W. Jones, G.H. Mahmud, Experimental test methods to determine the uniaxial tensile and compressive behaviour of ultra high performance fibre reinforced concrete (UHPFRC), Constr. Build. Mater. 37 (2012) 874–882, https://doi.org/10.1016/J.CONBUILDMAT.2012.04.030.
[51] P. Rossi, A. Arca, E. Parant, P. Fakhri, Bending and compressive behaviours of a new cement composite, Cem. Concr. Res. 35 (2005) 27–33, https://doi.org/10.1016/J.CEMCONRES.2004.05.043.
[52] E. Denarié, K. Habel, J. Wuest, SAMARIS deliverable D13, report on preliminary studies for the use of HPFRCC for the rehabilitation of road infrastructure components, http://samaris.zag.si, (2004).
[53] S.A.A.M. Fennis, J.C. Walraven, J.A. den Uijl, Compaction-interaction packing model: regarding the effect of fillers in concrete mixture design, Mater. Struct. 46 (2013) 463–478, https://doi.org/10.1617/s11527-012-9910-6.
[54] A. Hajiesmaeili, E. Denarié, Next generation UHPFRC for sustainable structural applications, Am. Concr. Inst. 326 (2018) 58.1–58.10.
[55] M.A. Hafiz, E. Denarié, Experimental study of tensile response of strain hardening UHPFRC at early age, Strain-hardening Cem. Compos, Springer, Dresden, Germany, 2018, pp. 308–315.
[56] M.A. Hafiz, E. Denarié, Tensile viscous response of Strain Hardening UHPFRC under high restraint and isothermal conditions, Euro C - 2018 Comput. Model. Concr. Struct, 2018, pp. 903–912.
[57] Standard Test Method for Flow of Hydraulic Cement Mortar BT - Standard Test Method for Flow of Hydraulic Cement Mortar, (15AD).
[58] SIA (2017), Cahier Technique 2052, Béton fibré ultra-performant (BFUP): Matériaux, dimensionnement et exécution, SIA, Zürich., (2017).
[59] G. Guignet, H. Kazemi-Kamyab, E. Denarié, Internal communication, August 2014, EPFL, Switzerland, 2014.
[60] S. Kolluru, J. Popovics, S.P. Shah, Determining elastic properties of concrete using vibrational resonance frequencies of standard test cylinders, Cem. Concr. Aggregates. 22 (2000) 81.
[61] L. Wadsö, Operational issues in isothermal calorimetry, Cem. Concr. Res. 40 (2010) 1129–1137 https://doi.org/10.1016/j.cemconres.2010.03.017.
[62] K. Scrivener, R. Snellings, B. Lothenbach, A Practical Guide to Microstructural Analysis of Cementitious Materials, Crc Press, 2018.
[63] O. Bjontegaard, Thermal Dilatation and Autogenous Deformation as Driving Forces to Self-induced Stresses in High Performance Concrete, Doctoral thesis The University of Trondheim, Norway, 1999.
[64] K. Kovler, Testing system for determining the mechanical behaviour of early age concrete under restrained and free uniaxial shrinkage, Mater. Struct. 27 (1994) 324–330.
[65] J.P. Charron, Contribution à l'étude du comportement au jeune âge des matériaux cimentaires en conditions de déformations libre et restreinte, Doctoral thesis University of Laval, Québec, Canada, 2003.
[66] M. Bouasker, N.E.H. Khalifa, P. Mounanga, N. Ben Kahla, Early-age deformation and autogenous cracking risk of slag–limestone filler-cement blended binders, Constr. Build. Mater. 55 (2014) 158–167.
[67] I. Mehdipour, K.H. Khayat, Elucidating the role of supplementary cementitious materials on shrinkage and restrained-shrinkage cracking of flowable eco-concrete, J. Mater. Civ. Eng. ASCE (2018) 30.
[68] P. Mounanga, M.I.A. Khokhar, R. El Hachem, A. Loukili, Improvement of the early-age reactivity of fly ash and blast furnace slag cementitious systems using limestone filler, Mater. Struct. 44 (2011) 437–453.
[69] Y. Ballim, P.C. Graham, The effects of supplementary cementing materials in modifying the heat of hydration of concrete, Mater. Struct. 42 (2009) 803–811.
[70] W. Huang, H. Kazemi-Kamyab, W. Sun, K. Scrivener, Effect of cement substitution by limestone on the hydration and microstructural development of ultra-high performance concrete (UHPC), Cem. Concr. Compos. 77 (2017) 86–101.
[71] P. Acker, Micromechanical analysis of creep and shrinkage mechanisms, Cocreep-6 Creep, Shrinkage Durab. Mech. Concr. Other Quasi-Brittle Mater, 2001, pp. 15–25.
[72] P. Acker, Why Does Ultrahigh-performance Concrete (UHPC) Exhibit Such Low Shrinkage and Such Low Creep? Spec. Publ. (2004), pp. 141–154.
[73] C. Hua, P. Acker, A. Ehrlacher, Analyses and models of the autogenous shrinkage of hardening cement paste: I. Modelling at macroscopic scale, Cem. Concr. Res. 25 (1995) 1457–1468.
[74] A. Bentur, K. Kovler, Evaluation of early age cracking characteristics in cementitious systems, Mater. Struct. 36 (2003) 183–190.
[75] J.P. Charron, J. Marchand, M. Pigeon, B. Bissonnette, Test device for studying the early-age stresses and strains in concrete, Spec. Publ, vol. 220, (2004), pp. 113–124, https://doi.org/10.14359/13153.